

Article

Cucumber (*Cucumis sativus* L.) Leaf Extract as a Green Corrosion Inhibitor for Carbon Steel in Acidic Solution: Electrochemical, Functional and Molecular Analysis

Lijuan Feng ^{1,*} , Shanshan Zhang ¹, Long Hao ² , Hongchen Du ¹, Rongkai Pan ¹, Guofu Huang ¹ and Haijian Liu ¹

- ¹ Shandong Engineering Research Center of Green and High-Value Marine Fine Chemical, Weifang University of Science and Technology, Weifang 262700, China; zhangshanshan87@wfust.edu.cn (S.Z.); duhongchen123@126.com (H.D.); panrk@wfust.edu.cn (R.P.); hgflh007@wfust.edu.cn (G.H.); liuhaijian.1987@163.com (H.L.)
- ² CAS Key Laboratory of Nuclear Materials and Safety Assessment, Institute of Metal Research, Chinese Academy of Sciences, Shenyang 110016, China; chinahaolong@126.com
- * Correspondence: ljfeng@alum.imr.ac.cn; Tel.: +86-053-6510-7638

Abstract: An extract of cucumber leaves (ECSL) was prepared as a green corrosion inhibitor for carbon steel. Its carbon steel corrosion inhibition performance against 0.5 mol L⁻¹ H₂SO₄ was investigated using electrochemical methods and scanning electron microscopy (SEM). Its composition was analyzed by gas chromatography and mass spectroscopy (GC–MS). Quantum chemical calculations and molecular dynamics simulations (MDS) were conducted to elucidate the adsorption mechanism of the inhibitor molecules on the carbon steel surface. The results indicated that the inhibition efficiency increases with its increasing concentration. The extract acted as a mixed type corrosion inhibitor, and its inhibition properties were ascribed to the geometric coverage effect induced by its adsorption on the metal surface in accordance with Langmuir’s law. The active components in the extract were identified as mainly organic compounds with functional groups such as aromatic moieties and heteroatoms. The inhibition activities of ECSL are delivered through the ability of the active components to adsorb on the metal surface through their functional groups to form a protective layer which hinders the contact of aggressive substances with carbon steel and thus suppresses its corrosion. This research provides an important reference for the design of green corrosion inhibitors based on plant waste materials.

Keywords: carbon steel; extract; green corrosion inhibitor; quantum chemical calculation



Citation: Feng, L.; Zhang, S.; Hao, L.; Du, H.; Pan, R.; Huang, G.; Liu, H. Cucumber (*Cucumis sativus* L.) Leaf Extract as a Green Corrosion Inhibitor for Carbon Steel in Acidic Solution: Electrochemical, Functional and Molecular Analysis. *Molecules* **2022**, *27*, 3826. <https://doi.org/10.3390/molecules27123826>

Academic Editor: Bogumil E. Brycki

Received: 12 April 2022

Accepted: 13 June 2022

Published: 14 June 2022

Publisher’s Note: MDPI stays neutral with regard to jurisdictional claims in published maps and institutional affiliations.



Copyright: © 2022 by the authors. Licensee MDPI, Basel, Switzerland. This article is an open access article distributed under the terms and conditions of the Creative Commons Attribution (CC BY) license (<https://creativecommons.org/licenses/by/4.0/>).

1. Introduction

As one of the basic industrial materials, carbon steel has been widely applied in various fields due to its excellent mechanical properties and low cost [1–8]. Nevertheless, it is prone to suffer from scale and corrosion due to its chemical and electrochemical interactions with the surrounding environment—which leads to the degradation of metallic structures [3,9–12]. Every year, a large amount of carbon steel equipment is damaged and replaced owing to metal corrosion, causing enormous economic losses and huge potential safety risks [13]. The most widely applied method for removing scale during facility maintenance activities is pickling [14,15]. Sulfuric acid is one of the most commonly used pickling agents, as it can effectively remove dirt and oxidation products from the metal surface [15–17]. However, the corrosion rate of carbon steel is so high in acidic conditions that the equipment may be damaged during the acidic cleaning process. Therefore, applying corrosion inhibitors is considered to be an unavoidable approach, and has been proven to be a convenient, effective and economical technique for protecting metals during such processes [5,11]. It has been revealed that organic compounds containing

heteroatoms, unsaturated bonds and planer conjugated systems usually display excellent corrosion inhibition activities because they adsorb onto the metal surface via their functional groups and form a protective film [3,5,18,19]. Unfortunately, traditional inhibitors are often toxic to human beings or have a detrimental impact on the environment, and so their use has been limited by more and more countries. Thus, researchers are keen to develop environmentally benign “green” corrosion inhibitors [3,10–14,20–26]. A perusal read of the literature has revealed that green inhibitors prepared from plant extracts are readily available, nontoxic, biodegradable and economical, and can be considered to be a most promising choice [16,23–26].

Cucumber (*Cucumis sativus* L.) is a vegetable that is widely planted in many countries. Its leaves are generally recognized as a biological waste material, causing serious ecological and environmental pollution. Meanwhile, it has been found that there are many valuable chemical constituents, including alkanoids, flavonoids, carbohydrates, proteins, sugars and steroids, in the leaves of plants [20,27–30]. These organic compounds contain adsorption centers—polar functional groups with N, S and O atoms or aromatic rings—in their molecular structures, which suggests that leaf extracts could be potential corrosion inhibitors [12,25,29–32]. However, there is no report to date on the corrosion inhibition performance of an extract based on cucumber leaves. Thus, if a corrosion inhibitor can be prepared from cucumber leaves, and if its corrosion inhibition mechanism can be determined, it will not only add a cheap new green product to the corrosion inhibitors list, but it will also provide a novel solution for the utilization of plant waste such as cucumber leaves. Therefore, in this study, an extract of cucumber leaves (ECSL) was prepared using an impregnation method, and its corrosion inhibition performance on carbon steel subjected to 0.5 mol L⁻¹ H₂SO₄ solution was evaluated through electrochemical measurements and surface analysis techniques. The active components of the extract were analyzed using gas chromatography and mass spectrometry. The adsorption performance of the active constituents on the surface of carbon steel was further revealed through theoretical calculations and simulations. The aims of the work were to assess the corrosion inhibition effects of the biological waste product; to reveal its inhibition mechanisms; to pave a way for the application of low-cost green plant extracts; and to promote the realization of resources recycling.

2. Results

ECSL was prepared as described in “Materials and Methods”, Section 3. Based on the experimental and theoretical analysis methods described in Section 3, the results are shown and discussed as follows.

2.1. Potentiodynamic Polarization Curves

Potentiodynamic polarization curves obtained from immersing the electrodes in 0.5 mol L⁻¹ H₂SO₄ solution with and without various concentrations of ECSL are shown in Figure 1. Curve fitting results obtained by Tafel extrapolation are shown in Table 1, where E_{corr} denotes the free corrosion potential; i_{corr} , the corrosion current density; β_c , the cathodic Tafel slope; and β_a , the anodic Tafel slope.

IE stands for the inhibition efficiency, which can be calculated according to the following equation:

$$IE (\%) = (i_{\text{corr}}^0 - i_{\text{corr}}) / i_{\text{corr}}^0 \times 100\% \quad (1)$$

where i_{corr}^0 and i_{corr} are corrosion current densities for the uninhibited and inhibited samples, respectively [5].

It can be seen from Figure 1 and Table 1 that the addition of ECSL led to both the anodic and cathodic branches of the polarization curves moving toward lower current density directions, indicating that both the anodic and cathodic reactions were inhibited by ECSL [33,34]. Moreover, the corrosion current reduced with an increasing concentration of ECSL, suggesting that the more inhibitor molecules that were adsorbed on the sample surface, the more the contact between the metal surface and the corrosion medium was

blocked. However, the changes in the anodic and cathodic Tafel slopes were very small, and the fluctuation of the corrosion potential was much less than 85 mV. Thus, it could be inferred that ECSL acted as a mixed type inhibitor which inhibited carbon steel corrosion by forming a protective structure, obstructing both the anodic and cathodic electrochemical reactions of the corrosion process [5,35,36].

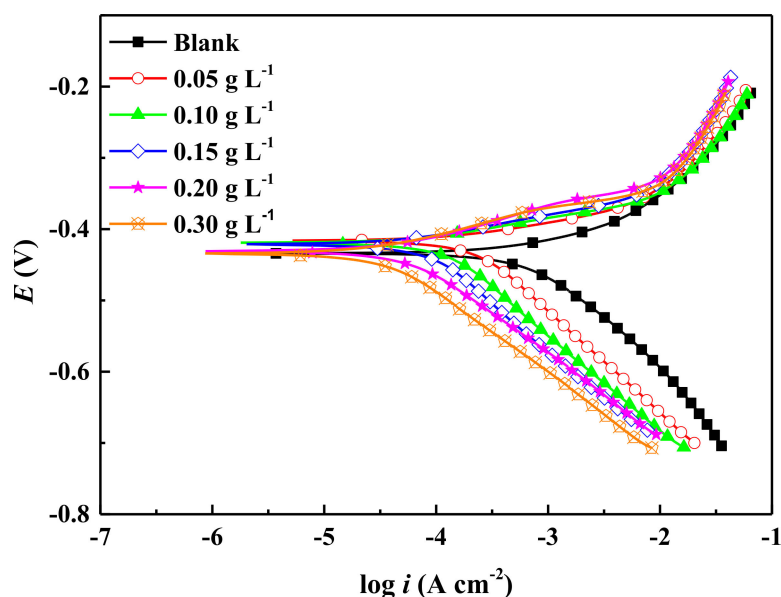


Figure 1. Potentiodynamic polarization curves of the carbon steel samples in $0.5 \text{ mol L}^{-1} \text{ H}_2\text{SO}_4$ solution with and without different concentrations of ECSL.

Table 1. Curve fitting results for the potentiodynamic polarization curves for carbon steel in $0.5 \text{ mol L}^{-1} \text{ H}_2\text{SO}_4$ solution with and without different concentrations of ECSL.

$C_{\text{inh}} \text{ (g L}^{-1}\text{)}$	$\beta_a \text{ (mV dec}^{-1}\text{)}$	$\beta_c \text{ (mV dec}^{-1}\text{)}$	$i_{\text{corr}} \text{ (mA cm}^{-2}\text{)}$	$E_{\text{corr}} \text{ (mV)}$	$IE \text{ (\%)}$
0	58	125	0.73	−430	/
0.05	59	127	0.35	−420	51.7
0.10	59	126	0.19	−419	73.8
0.15	60	127	0.13	−422	82.1
0.20	61	127	0.066	−431	90.9
0.30	62	130	0.047	−434	93.5

2.2. Electrochemical Impedance Spectroscopy (EIS) Measurements

Figure 2 shows the electrochemical impedance spectrum for carbon steel electrodes in $0.5 \text{ mol L}^{-1} \text{ H}_2\text{SO}_4$ solution with and without various concentrations of ECSL. It is obvious that only one capacity loop appeared in the Nyquist diagram for all electrodes, indicating that the carbon steel corrosion was mainly controlled by the charge transfer reaction [37]. However, the impedance behavior of the carbon steel sample was significantly changed by the presence of ECSL. It is notable that the radius of the capacitive loop enlarged with increasing ECSL concentration, suggesting that the anti-corrosion properties were gradually enhanced due to the increasing surface coverage of the electrode with increasing inhibitor concentration [33]. The EIS activities for the carbon steel samples in acidic solution, either with or without ECSL, can be interpreted using a model that describes a solution resistor element connecting with a unit of charge transfer resistor and double layer capacitor in parallel $[R(QR)$ equivalent circuit], as shown in Figure 3; where R_s represents the solution resistance, R_{ct} the charge transfer resistance and C_f the capacitance of the double electric layer. Since all the capacitive semicircles were depressed (Figure 2), the constant phase element CPE (Q) was used to replace C for the description of the frequency independent

phase shift induced by the roughness of the electrode surface [38,39]. The value of CPE can be assessed using the following equation:

$$Z(\omega) = (Z_0)^{-1} (j\omega)^{-n} \tag{2}$$

where Z_0 is the CPE constant, ω is the angular frequency (in rad/s), $j^2 = -1$, is the imaginary number and n is the CPE exponent. Depending on n , CPE can represent resistance [$Z(\text{CPE}) = R, n = 0$], capacitance [$Z(\text{CPE}) = C, n = 1$], inductance [$Z(\text{CPE}) = L, n = -1$] or Warburg impedance (for $n = 0.5$). Thus, the inhibition efficiency can be calculated from the following formula:

$$\eta (\%) = \theta (\%) = (1 - R_{ct}/R_{ct}^0) \times 100\% \tag{3}$$

where η denotes the inhibition efficiency and θ indicates the surface coverage [40–42]. The curve fitting results based on the $R(QR)$ circuit are displayed in Table 2.

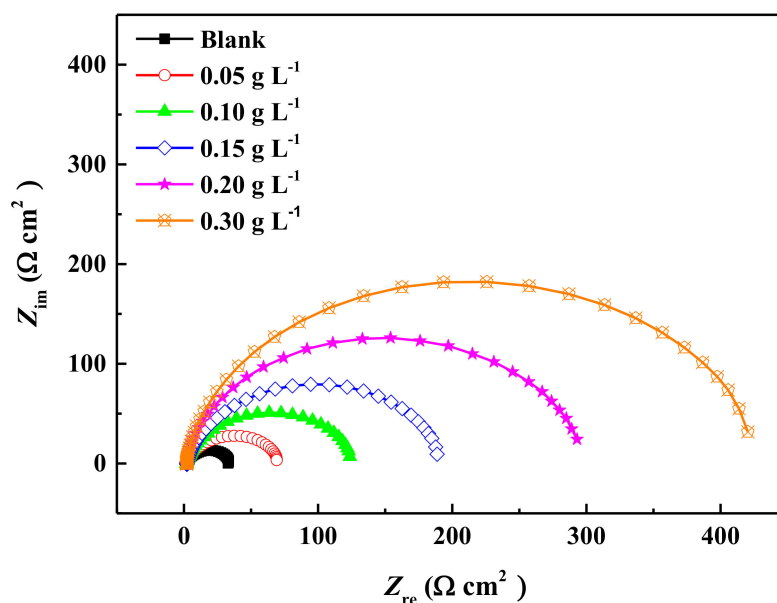


Figure 2. Electrochemical impedance spectrum of carbon steel samples in 0.5 mol L⁻¹ H₂SO₄ solution with and without different concentrations of ECSL.

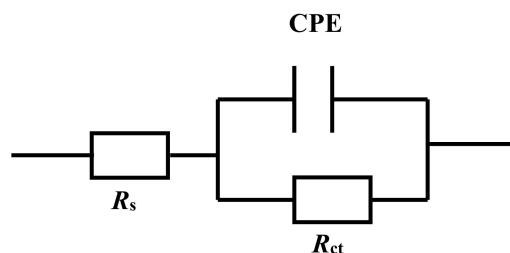


Figure 3. Equivalent circuit to fit the impedance data for carbon steel in 0.5 mol L⁻¹ H₂SO₄ solution with and without different concentrations of ECSL.

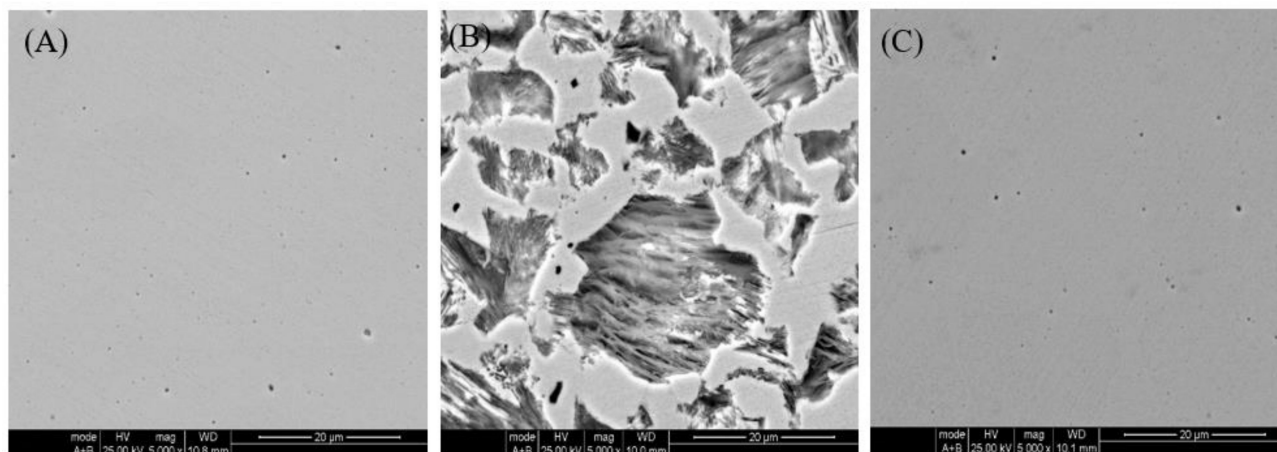
Based on Table 2, the capacity of the electrode was decreased in the presence of ECSL; this is ascribed to the fact that the acidic solution with its larger dielectric constant was replaced by the extract molecules with a smaller dielectric constant, which improved the double layer structure [43,44]. As the concentration of the inhibitor was increased, the double layer became thicker, reducing the local dielectric constant; which led to a decrease in the double layer capacity [45]. Meanwhile, the charge transfer resistance increased with increasing inhibitor concentration, indicating increasing mitigation of electrochemical corrosion. This is because the active molecules in ECSL were adsorbed onto the carbon steel surface and the charge transfer process was reduced, causing a corrosion inhibition effect.

Table 2. Curve fitting results of the electrochemical impedance data for carbon steel in 0.5 mol L⁻¹ H₂SO₄ solution with and without different concentrations of ECSL.

C_{inh} (g L ⁻¹)	R_s (Ω cm ²)	CPE-C (μ F cm ⁻²)	CPE-n	R_{ct} (Ω cm ²)	η (%)
0	1.94	104	0.95	29.3	/
0.05	2.22	86.6	0.94	62.9	53.4
0.10	2.19	62.2	0.94	118	75.2
0.15	1.97	51.8	0.94	147	80.1
0.20	2.11	43.6	0.94	281	89.6
0.30	2.01	33.9	0.94	406	92.8

2.3. Scanning Electron Microscopy (SEM) Observations

SEM observations were conducted with the aim of confirming the changes in the surface morphologies of carbon steel samples before and after the addition of ECSL. Figure 4 depicts the SEM images of samples immersed in 0.5 mol L⁻¹ H₂SO₄ solution in the absence and presence of ECSL. For comparison purposes, an image of the morphology of the sample before immersion is also included. It is clear that many large holes appeared in the surface of the sample immersed in acid without ECSL, indicating that the surface of the carbon steel was seriously damaged and the sample suffered from serious corrosion. In the presence of ECSL, however, the surface of the sample was smooth, with only a few slight scratches induced by emery papers visible. It had an appearance similar to that of the sample before immersion, suggesting corrosion of the carbon steel was significantly inhibited by the plant extract. This might be ascribed to the active constituents of ECSL interacting with the metal surface and forming a protective layer, decreasing the contact area of the sample with the aggressive medium and consequently mitigating its corrosion [27,46].

**Figure 4.** SEM images. (A) carbon steel sample before immersion; (B) carbon steel sample immersed in 0.5 mol L⁻¹ H₂SO₄ solution; (C) carbon steel sample immersed in 0.5 mol L⁻¹ H₂SO₄ solution with 0.20 g L⁻¹ ECSL.

2.4. Adsorption Isotherm

Previous researchers have confirmed that the adsorption behavior of organic molecules on metal surfaces has a decisive influence on their corrosion inhibition performance [47,48]. In order to further analyze the corrosion protection mechanism of ECSL, the surface coverage degree (θ) of different concentrations of the inhibitor was tested by fitting to several isotherms; the data fitted best with the Langmuir adsorption isotherm, as shown in Figure 5. According to Langmuir's adsorption isotherm law, the relationship between θ and C_{inh} is shown by the following equation:

$$C_{inh}/\theta = 1/K + C \quad (4)$$

where K represents the adsorption equilibrium constant, C_{inh} is the concentration of the extract, and θ is the surface coverage degree, which is approximately equal to η in Table 2 [5,49,50].

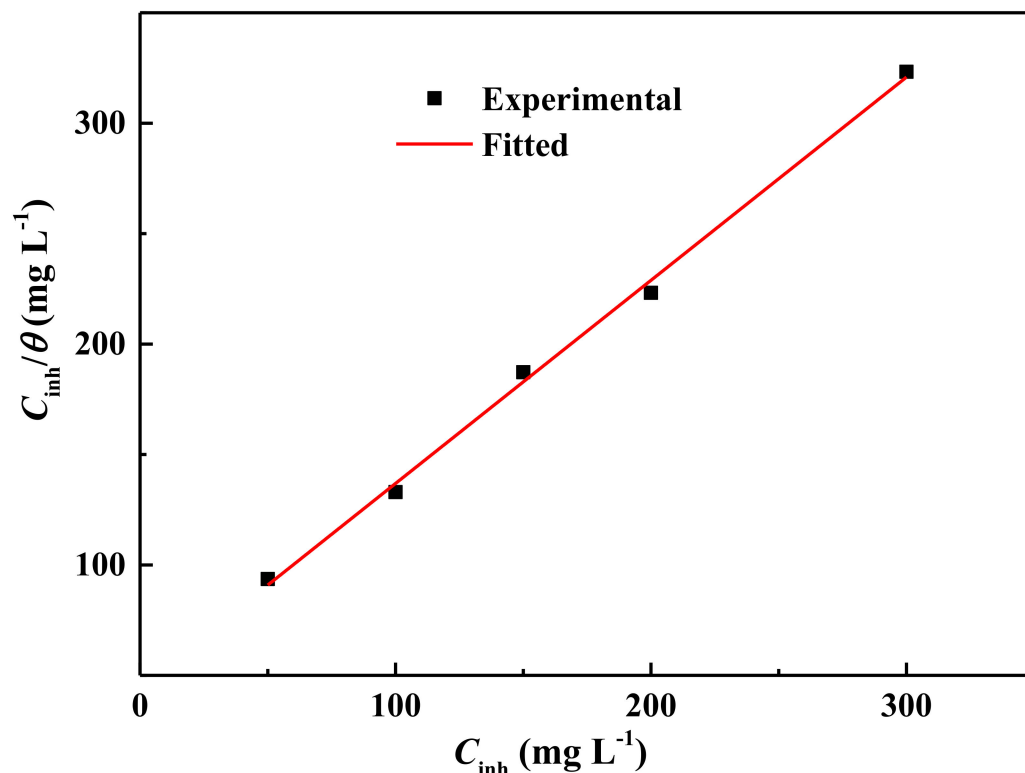


Figure 5. Langmuir adsorption isotherm for ECSL adsorbed on the carbon steel sample surface in $0.5 \text{ mol L}^{-1} \text{ H}_2\text{SO}_4$ solution.

It is clear from Figure 5 that C_{inh}/θ has a linear relationship with C_{inh} , with a slope close to 1. The linear coefficient was 99.9% and the adsorption equilibrium constant K was calculated to be approximately 22.3 L g^{-1} . This result indicated that the adsorption performance of ECSL on the carbon steel surface conformed to Langmuir's adsorption law, and that the corrosion inhibition mechanism was the geometric covering effect.

2.5. Gas Chromatography and Mass Spectroscopy (GC–MS) Analysis

In order to further reveal the reasons for its corrosion inhibition effects, the constituents of ECSL were analyzed by GC–MS. The spectrum obtained is depicted in Figure S1. After preliminary analysis, it was identified that there are more than forty substances present in the extract, of which eleven compounds were most likely to have corrosion inhibition effects. These eleven chemical constituents, along with their molecular formula, abbreviations, retention time and molecular weight are listed in Table 3. As can be seen in Figure S1 and Table 3, it is notable that ECSL contains a variety of organic substances with multiple functional groups, such as rings, double bonds, π bonds and heteroatoms. Based on previous theories, such compounds have extraordinary adsorption potential, and are very promising corrosion inhibitors as they favor an ability to adsorb on the metal surface using these groups as adsorption centers, and subsequently inhibit metal corrosion.

Table 3. Compounds identified from the GC–MS chromatogram, and molecular information assigned to the respective signals.

Name of the Compound	Abbreviation	Retention Time (min)	Molecular Formula	Molecular Weight
1-gala-l-ido-octose	GIO	1.737	C ₈ H ₁₆ O ₈	240
Topotecan	TO	2.215	C ₂₃ H ₂₃ N ₃ O ₅	421
Styrene	ST	8.616	C ₈ H ₈	104
2-ethyl-1-hexanol	EH	13.14	C ₈ H ₁₈ O	130
2-amino-5-[(2-carboxy)vinyl]-imidazole	IACV	15.24	C ₆ H ₇ N ₃ O ₂	153
Adrenalone	AD	19.62	C ₉ H ₁₁ NO ₃	181
Benzocycloheptatriene	BT	22.02	C ₁₁ H ₁₀	142
Actinobolin	AC	24.73	C ₁₃ H ₂₀ N ₂ O ₆	300
Pterin-6-carboxylic acid	PCA	27.37	C ₇ H ₅ N ₅ O ₃	207
2,5-difluoro-β, 3, 4-trihydroxy-N-methyl-benzeneethanamine	BDTM	30.74	C ₈ H ₁₁ F ₂ N	219
4'-methyl-2-hydroxystilbene	MH	33.26	C ₁₅ H ₁₄ O	210

2.6. Quantum Chemical Calculations

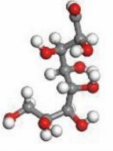
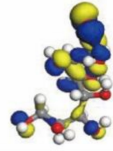
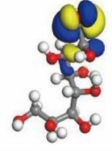
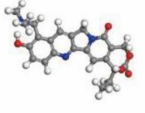
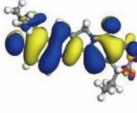
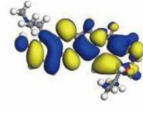
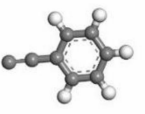
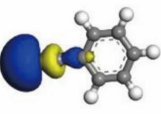
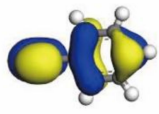
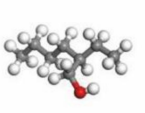
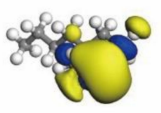
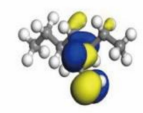
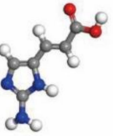
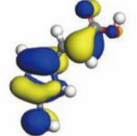
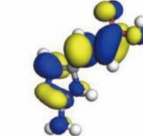
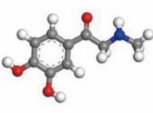
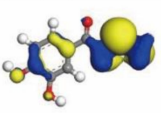
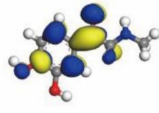
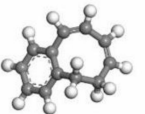
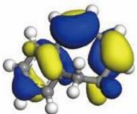
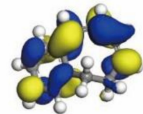
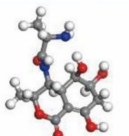
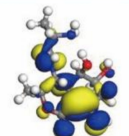
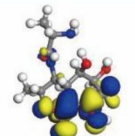
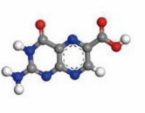
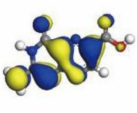
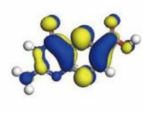
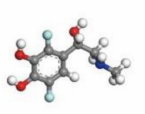
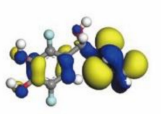
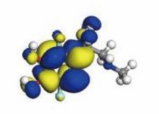
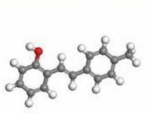
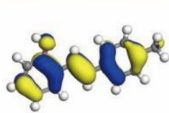
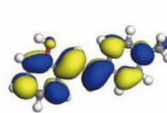
The corrosion activities of organic substances are closely related to their molecular, spatial and electronic structures. The adsorption of molecules mainly occurs relative to their frontier orbitals, namely, the highest occupied orbital (HOMO) and the lowest occupied orbital (LUMO). Further, their adsorption properties depend on the energy of the HOMO (E_{HOMO}) and LUMO (E_{LUMO}) [51–53]. The higher the E_{HOMO} of the molecule, the more difficult it is for the nucleus to attract electrons to its orbital, and therefore, the easier it is to donate electrons to form coordination bonds with the unoccupied orbital. The lower E_{LUMO} of the molecule, the easier it is to accept electrons and form feedback bonds. The difference in energy between the LUMO and HOMO ($\Delta E = E_{\text{LUMO}} - E_{\text{HOMO}}$) is also an important parameter to describe the reactivity of the inhibitor molecule toward the surface, if the difference in electronegativity between the molecule and the metal cannot be ignored [54]. In such cases, a higher ΔE suggests better stability of the molecule, and it will be more difficult for the molecule to participate in the adsorption reaction. In contrast, a lower ΔE indicates that it is easier to adsorb the molecule onto the metal surface to construct a protective film [21,55]. Generally, the effect on the molecular adsorption performance of a molecule at the metal surface is reflected in the parameter of global hardness (H).

Figure 6 depicts the optimized molecular structures, and the HOMO and LUMO distributions of the eleven identified components. The locations of the HOMO and LUMO analyzed from the data in Figure 6 are shown in Table 4. Due to the density functional theory (DFT) not being suitable for computing the ionization potential and the electron affinity based on Koopman's theorem [54–56], the Hartree–Fock (HF) method was subsequently used to calculate the values of E_{LUMO} , E_{HOMO} , ΔE and other quantum chemical parameters elucidated from E_{LUMO} and E_{HOMO} .

According to Koopman's theorem, the ionization potential (I) and the electron affinity (A) can be determined using the following equations, respectively:

$$I = -E_{\text{HOMO}} \quad (5)$$

$$A = -E_{\text{LUMO}} \quad (6)$$

Compound	Optimized Structure	HOMO	LUMO
GIO			
TO			
ST			
EH			
IACV			
AD			
BT			
AC			
PCA			
BDTM			
MH			

Legend: ● C; ● H; ● O; ● N; ● F.

Figure 6. Optimized molecular structures and frontier molecular orbital density distributions of the eleven compounds identified in ECSL.

Table 4. HOMO and LUMO distributions of compounds identified in ECSL.

Compound	HOMO Distribution	LUMO Distribution
GIO	O	O
TO	Rings	Rings
ST	C in the branch	Rings
EH	Branch with O atom	Branch with O atom
IACV	Pentatomic ring, O, N	Pentatomic ring, O, N
AD	Benzene ring, N, O	Benzene ring, N, O
BT	Rings	Rings
AC	Rings, N	Rings, N
PCA	Rings, O	Rings, O
BDTM	O, N, Benzene ring	O, Benzene ring
MH	Benzene rings	Benzene rings

The global hardness (H), the electronegativity (X) and the number of electrons transferred (ΔN) can be calculated according to the following relationships:

$$H = (I - A)/2 \quad (7)$$

$$X = (I + A)/2 \quad (8)$$

$$\Delta N = (X_{\text{Fe}} - X_{\text{inh}})/2(H_{\text{Fe}} - H_{\text{inh}}) \quad (9)$$

where $X_{\text{Fe}} = I_{\text{Fe}} = 7$ eV, and $H_{\text{Fe}} = 0$ for iron, based on Pearson's electronegativity scale assumption [57–59]. However, their application of $X_{\text{Fe}} = 7$ eV for the calculation of ΔN has been severely criticised because the value of 7 eV was obtained according to the free electron gas Fermi energy of iron using the free electron gas model. In that case, the electron–electron interaction is neglected, which causes differences from the state of the bulk metal, and therefore the use of this value is conceptually inappropriate. Thus, Kokalj suggested that the work function (Φ_{Fe}) be used to replace X_{Fe} . Hence, ΔN can be calculated as follows:

$$\Delta N = (\Phi_{\text{Fe}} - X_{\text{inh}})/2H_{\text{in}} \quad (10)$$

Considering that metal corrosion most likely occurs at the densely packed surface, $\Phi_{\text{Fe}} = 5.07$ V obtained from the experimental result was applied to calculate ΔN [55,60]. The resulting structural parameters are listed in Table 5.

Table 5. Quantum chemical parameters of active components identified in ECSL.

Compound	E_{HOMO} (eV)	E_{LUMO} (eV)	ΔE (eV)	H (eV)	X (eV)	ΔN
GIO	−11.03	2.66	13.69	6.85	4.18	0.07
TO	−8.17	1.09	9.25	4.63	3.54	0.17
ST	−8.39	2.65	11.04	5.52	2.87	0.20
EH	−11.33	3.74	15.07	7.53	3.79	0.08
IACV	−7.80	2.35	10.14	5.07	2.72	0.23
AD	−8.64	2.42	11.05	5.53	3.11	0.18
BT	−8.09	2.60	10.69	5.35	2.75	0.22
AC	−9.09	2.75	11.83	5.92	3.17	0.16
PCA	−9.14	1.55	10.69	5.34	3.80	0.12
BDTM	−8.64	3.58	12.21	6.10	2.53	0.21
MH	−7.82	2.21	10.03	5.01	2.81	0.23

By carefully analyzing the data in Figure 6 and Table 4, we can elucidate that the HOMOs of the identified substances are mainly distributed in the aromatic rings (TO, AD, BT, BDTM, MH), heterocycles (TO, IACV, AC, PCA) and heteroatoms (GIO, TO, EH, IACV, AD, AC, BDTM, MH), which indicates that these sites have nucleophilic activities and are the preferred adsorption centers. Thus, the molecules can donate electrons to construct coordination bonds with iron and form a protective layer. The LUMOs of these substances

are also mainly in benzene rings (TO, ST, AD, BT, BDTM, MH), heterocycles (TO, IACV, AC, PCA), and heteroatoms (GIO, TO, EH, IACV, AD, AC, PCA, BDTM, MH), which suggests that these compounds can accept electrons from the vacant d orbital of a metal to constitute a feedback bond. Therefore, it is possible that the molecules in ECSL first physically adsorb onto the surface of carbon steel, and then chemically interact with it to form a protective structure trough, sharing electron pairs between the ECSL molecules and the iron [61].

From Table 5, the difference in electronegativity between the molecule and the metal is visible in comparing the value of X_{inh} with that of Φ_{Fe} ; thus, the influence of ΔE on the molecular adsorption properties should be considered [54]. Consequently, the global hardness parameter (H), closely related to ΔE , indicates the charge transfer resistance, which is directly proportional to the energy change, including both the charge transfer to the molecule and the back donation from the molecule [62,63]. This indicates the reactivity of the inhibitor molecule towards the adsorption on a metallic surface. Generally, the reactivity of the molecule increases as the value of H or ΔE decreases. Thus, the inhibition efficiency of the molecule increases, since it is more possible to form a bond-anti-bond structure through offering and accepting electrons to and from the metal [21]. The results in Table 5 show that TO displays the lowest value, 4.63 eV, which is ascribed to the fact that this molecule contains the most rings and multiple heteroatoms. Most of the compounds have H values ranging from 5.0 to 6.1 eV. These values of H are a little higher than those calculated via DFT. This is reasonable since the H value calculated through DFT is lower than that found using the HF method, which has been confirmed by the studies of other researchers [57,64,65]. Accounting for the applicable condition of Koopman's theorem, the H value obtained by the HF method is more reliable, and an H value in the range from 5.0 to 6.1 eV is suitable for a molecule with an inhibition effect [55,66,67]. In combination with Figure 6 and Table 4, these data indicate that these molecules all contain ring structures (benzene moiety or heterocyclic) with dislocation electrons. In terms of HSAB (hard/soft-acid/base) theory, these compounds can be recognized as soft bases which react with soft acids [68,69]. The H values of GIO and EH are the highest (6.85 and 7.53 eV, respectively) due to the fact that they only get negatively charged atoms and do not have conjugated structures. These two compounds can be recognized as hard bases. The inhibition effect of ECSL might be enhanced by the different types of compounds present. In the Fe–H₂O system, there are different Lewis acids on the metal surface: the bare iron is categorized as a soft acid and the metal ions produced in the corrosion process are hard acids [70]. Soft bases such as TO can interact directly with the surface of the iron and form an adsorption film, protecting the metal from corrosion. EH and GIO, as hard bases, can interact with the Fe³⁺ or Fe²⁺ ions and assist the inhibition performance.

Electronegativity (X) reflects the ability of atoms to attract electrons toward themselves, and can be used to assess the tendency of a molecule to retain its own electrons during donor/acceptor interactions that lead to corrosion inhibition [59,62]. Usually, a compound with a lower value of X means that it shares electrons with metals more easily, and can be expected to have higher inhibition performance [59,71]. From Table 5, there are four compounds (GIO, EH, TO and PCA) with an X value higher than 3.5 eV. Considering that GIO and EH are also the molecules with the highest H values, such high X values suggest they interact with the metal solely via a physical electrostatic effect, rather than by the chemical reaction of donating electrons. PCA and TO also have the lowest E_{LUMO} , indicating that they are more likely to be electron acceptors rather than donors during their interaction with metals. The X values of the other seven substances have no significant differences, which may be ascribed to the fact that they all have planar ring structures with conjugated π bonds. Thereby, when they interact with metals, they are probably able to offer both electrons to the empty orbital of a metal molecule and receive electrons to form back-donation bonds, and as a result, they can strongly adsorb on the metal surface and constitute a protective layer, inhibiting its corrosion.

The fraction number of electrons transferred (ΔN) indicates inhibition efficiency resulting from electron donation [57]. If $\Delta N > 0$, electrons can be transferred from organic

molecules to metals and form feedback (back-donation) bonds. If $\Delta N < 3.6$, the inhibition efficiency increases with increasing ability to donate electrons to the metal surface [61,72]. Per Table 5, the ΔN values of all the compounds are in the range from 0 to 3.6, revealing that they can interact with the metal via electron donation from the inhibitor to the metal surface.

2.7. Molecular Dynamics Simulations (MDS)

Molecular dynamics simulation is a comprehensive technology that combines mathematics, chemistry and physics through computational simulations to calculate the properties of materials in the system [61,71–73]. In order to better understand the interaction between ECSL and the carbon steel surface, and furthermore, to elucidate its corrosion inhibition mechanism, MDS was performed to analyze the adsorption behaviors of the active components of ECSL on the Fe(110) surface at the molecular level.

The optimized adsorption configurations of the molecular structures on the metal surface are illustrated in Figure 7. The adsorption configuration of each molecule on the Fe(110) surface in $0.5 \text{ mol L}^{-1} \text{ H}_2\text{SO}_4$ solution can be vividly observed by comprehensive analysis of Figures 6 and 7, and Table 5. The GIO molecule adsorbs on the iron surface with the O atoms on its one side supporting like feet. TO adsorbs on the Fe(110) surface with the benzene rings and imidazole plane parallel to it. ST adsorbs with its benzene ring parallel to the Fe(110) surface and its hydrophobic carbon chain tilting upward. EH adsorbs using the O atom as the adsorption center with a C atom assisting. The adsorption centers of IACV are an imidazole ring as well as the O atoms; while those of AD are O atoms and the benzene ring. As to the adsorption of BT, the benzene ring is parallel to the Fe(110) surface, with the C atom supported on one side. AC adsorbs with the aromatic moieties parallel to the metal surface; meanwhile, the N and O atoms serve as adsorption centers to strengthen its adsorption. The PCA molecule horizontally adsorbs on the Fe(110) surface through the double ring structure, while the O and N atoms of the branched chain can also perform as active adsorption centers, which facilitates its adsorption. Due to space configuration constraints, BDTM adsorbs on the metal surface at a certain angle, yet its heteroatoms can still act as the adsorption centers. MH molecules adsorb mainly through their benzene rings.

In general, by careful examination of Figure 7, it can be noted that all eleven compounds identified in ECSL are able to adsorb on the Fe(110) surface, therefore a barrier structure can be formed to isolate contact between the carbon steel surface and the corrosive medium, thus mitigating the corrosion of the carbon steel.

It should be mentioned that, owing to spatial structure limitations, the adsorption configuration of an organic molecule on a metal surface is not the same as the optimal geometric structure obtained by quantum chemical calculations; instead, it is adjusted to a certain extent. As a result, the distance from the metal surface to the adsorbed molecules varies. As shown in Figure 7, for molecules with less active groups, like EH and GIO, the distance between the molecule and the metal surface is obviously larger than that of other molecules. In fact, the high values (3.916 and 3.916 Å, respectively) indicate their interactions with the metal are through physical adsorption mechanisms rather than chemical ones [55]. Compounds containing planer moieties, especially benzene rings, interact easily with the metal and can adsorb onto the Fe(110) surface at a short distance, since the planer structure can be parallel to the Fe(110) surface. ST, IACV, AD, PCA, BDTM and MH all display such adsorption configurations. However, if the branched chains in the molecule are too many or too long, and they cannot adjust to the same side of the planar structure, such as in BT and AC, the molecule will not adsorb on the metal surface so closely. These results are expected to provide a reference for the design of new high-efficiency corrosion inhibitors.

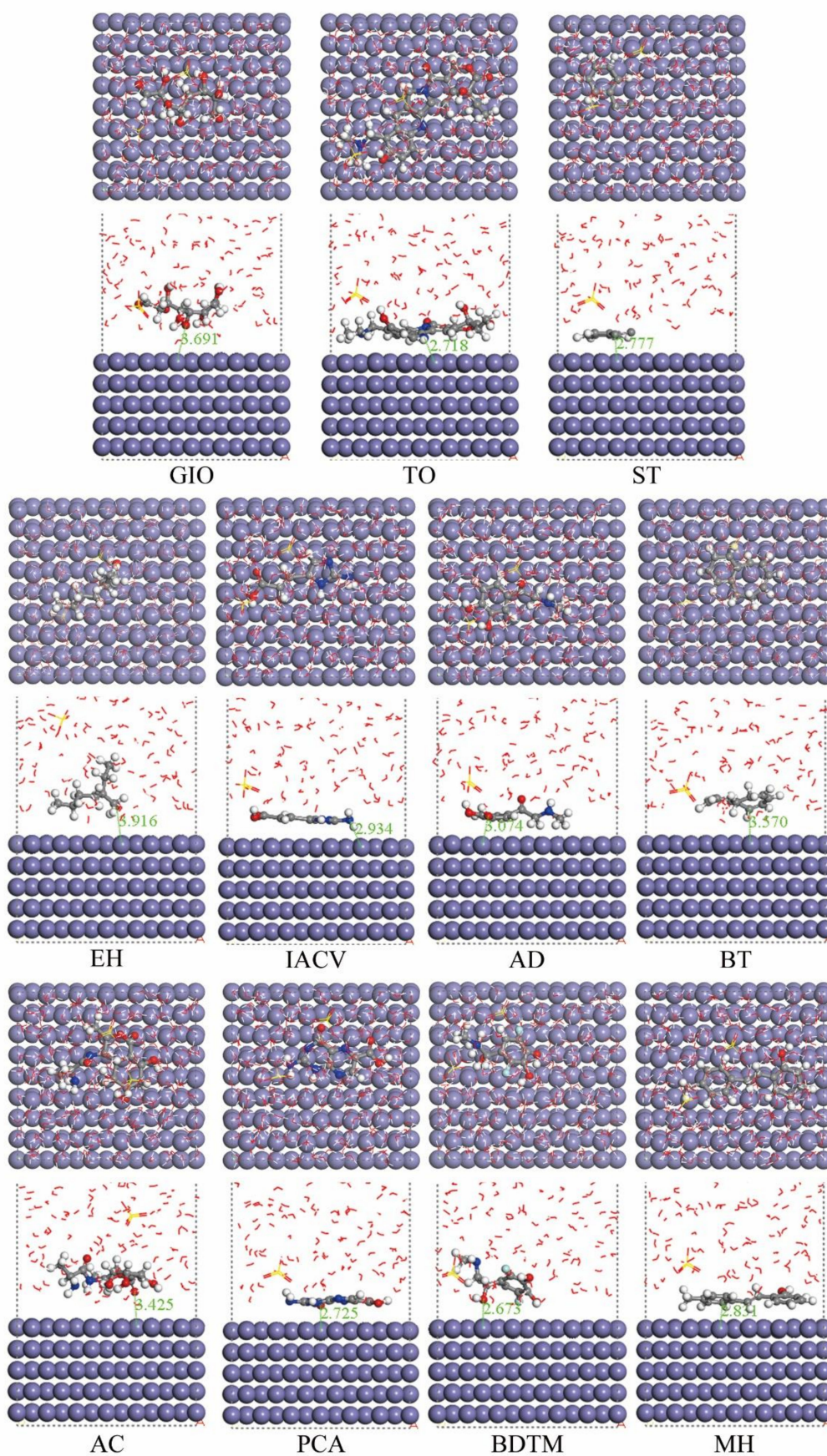


Figure 7. Optimized adsorption configurations of the molecular structures on Fe(110) surface.

The adsorption energy (E_{ads}) between the iron surface and the organic compound can be calculated as follows:

$$E_{\text{ads}} = E_{\text{total}} - (E_{\text{surf+solu}} + E_{\text{inh}}) \quad (11)$$

where E_{total} is the total energy of the inhibitor molecule adsorption system on the Fe(110) surface in 0.5 mol L⁻¹ H₂SO₄ solution, and $E_{\text{surf+solu}} + E_{\text{inh}}$ is the sum of the energy including the metal surface, the corrosive solution and the inhibitor molecule before adsorption [72,74]. The calculated results are listed in Table 6 from the lowest to the highest adsorption energy value. It has been acknowledged that a negative adsorption energy value indicates spontaneous adsorption of a molecule on a metal surface. Moreover, a lower value of E_{ads} implies the molecule is more likely to adsorb on the metal surface, thus, it exhibits a better corrosion inhibition performance [58,59]. It can be observed from Table 6 that the adsorption energy on the Fe(110) surface for each molecule has a negative value, indicating that all eleven components identified in ECSL are able to adsorb on the carbon steel surface and exhibit corrosion inhibition effects.

Table 6. Interaction energies for each component identified in ECSL with Fe(110) surface.

Compound	$E_{\text{surf+solu}} + E_{\text{inh}}$ (kcal mol ⁻¹)	E_{total} (kcal mol ⁻¹)	E_{ads} (kcal mol ⁻¹)
TO	-30,302.11	-31,204.32	-902.21
PCA	-30,444.21	-31,331.86	-887.65
BDTM	-30,397.84	-31,277.37	-879.53
AC	-30,430.67	-31,246.72	-816.05
AD	-30,390.48	-31,200.68	-810.19
ST	-30,001.78	-30,759.53	-757.75
IACV	-30,570.80	-31,195.94	-625.14
MH	-30,411.15	-31,000.90	-589.75
BT	-30,353.40	-30,924.26	-570.86
GIO	-30,351.34	-30,850.19	-498.85
EH	-30,431.33	-30,870.30	-438.97

2.8. Corrosion Inhibition Mechanism

The corrosion inhibition mechanism of ECSL for carbon steel can be analyzed from the chemical structures of the identified components. The main chemical constituents of ECSL are organic compounds containing many functional groups, such as benzene rings, heterocycles and polar atoms, which have delocalized or unpaired electrons and demonstrate high E_{HOMO} . They are prone to provide electrons to the empty d orbital of Fe and adsorb on its surface. Meanwhile, by virtue of these functional groups, they have low E_{LUMO} and easily accept electrons from the d orbital of Fe to form feedback bonds and enhance the adsorption capacity. Thereby, the active components in ECSL can adsorb on the metal surface and constitute a protective structure. Moreover, ECSL contains a variety of active components, including both soft bases and hard bases, which can either directly adsorb on the carbon steel surface or interact with Fe²⁺ and/or Fe³⁺ to form a protective layer. Therefore, they complement each other, to a certain extent, to enhance the metal corrosion inhibition properties. As a result, ECSL can spontaneously and effectively adsorb on the carbon steel surface and inhibit its corrosion.

3. Materials and Methods

3.1. Materials

The metal samples were prepared from R235 carbon steel, which was machine cut into cuboid samples with the dimensions of 10 mm × 10 mm × 5 mm. The composition of the carbon steel is listed in Table 7. The sample was embedded in a PVC holder using epoxy resin, leaving only a working surface with an area of 1 cm² for electrochemical measurements. Prior to each experiment, the working surface was abraded with sandpaper from 100 to 1000 mesh, degreased with acetone, rinsed in distilled water, and air-dried. The

corrosive medium was $0.5 \text{ mol L}^{-1} \text{ H}_2\text{SO}_4$ solution which was prepared from analytical reagent grade H_2SO_4 and bi-distilled water.

Table 7. Composition of carbon steel in wt. (%).

Composition	C	Si	Mn	P	S	Fe
Amount (%)	0.16	0.14	0.48	0.03	0.03	99.16

3.2. ECSL Preparation

Fresh cucumber leaves (collected from the green house of the agricultural experimental base at Weifang University of Science and Technology, China) were cleaned under running water and then distilled water to remove the surface dirt. Next, the leaves were dried in an oven at $45 \text{ }^\circ\text{C}$ for approximately 24 h. The dried leaves were then ground to a powder and screened with a sieve with the pore size of 0.15 mm. After that, the dried and powdered cucumber leaves were soaked in ethanol (75% by volume) for 2 h at $25 \text{ }^\circ\text{C}$. Then, the plant extract was boiled at $45 \text{ }^\circ\text{C}$, naturally cooled to room temperature, and triple-filtered. The excess ethanol was removed by vacuum distillation. Finally, the plant extract, a dark brown solid residue, was obtained.

3.3. Chemical Composition Analysis

In order to identify the effective components of the plant extract, GC–MS analysis was carried out using Agilent Technologies GC model 7890A and Mass Spectrometry model 5977, coupled with an HP-5 capillary fused silica column of dimensions $30 \text{ } \mu\text{m} \times 320 \text{ } \mu\text{m} \times 0.25 \text{ } \mu\text{m}$. The carrier gas was helium, the pressure was controlled at 11.604 Psi and the flow rate was 1.5 mL min^{-1} . The oven temperature was programmed as follows: the initial temperature was set as $35 \text{ }^\circ\text{C}$ (isothermal for 5 min); then the temperature was increased to $90 \text{ }^\circ\text{C}$ at the rate of $6 \text{ }^\circ\text{C min}^{-1}$ (isothermal for 3 min); then to $150 \text{ }^\circ\text{C}$ at $5 \text{ }^\circ\text{C min}^{-1}$ (isothermal for 2 min); and finally, to $200 \text{ }^\circ\text{C}$ at $5 \text{ }^\circ\text{C min}^{-1}$ (isothermal for 3 min). All peaks were analyzed by matching with those in the NIST library to obtain the exact information.

3.4. Electrochemical Techniques

Electrochemical measurements were conducted using an electrochemical work station (CHI-660E, Chenhua) equipped with a three-electrode system, where the carbon steel sample served as the working electrode, a platinum plate as the auxiliary electrode and a saturated calomel electrode (SCE) as the reference electrode. The polarization curves were determined from a cathodic potential of -0.25 V to an anodic potential $+0.25 \text{ V}$, with respect to the open circuit potential (OCP), at a sweep rate of 1 mV s^{-1} . Electrochemical impedance spectroscopy (EIS) plots were acquired in the frequency range from 100 kHz to 10 mHz with a perturbation amplitude of 10 mV. The EIS spectra were fitted using the Corrview software. A fresh working electrode was used for each measurement. At least three runs were performed for each measurement to obtain reproducible data.

3.5. Surface Morphological Observation

The surface morphologies of the carbon steel samples immersed in $0.5 \text{ mol L}^{-1} \text{ H}_2\text{SO}_4$ solution for 2 h with and/or without 0.20 g L^{-1} ECSL were observed by scanning electron microscopy (SEM, Philip XL 30) at $5000\times$ magnification. The energy of the acceleration beam employed was 25 kV.

3.6. Computational Details

All of the quantum chemical calculations and molecular dynamics simulations were performed using Materials Studio 2019 software supplied by Biovia Community. The molecular structures of the inhibitors were fully geometrically optimized by DMol3 module using the function of PBE (proposed by Perdew–Burke–Ernzerhof) with the double numeric

basis set of DNP in the DFT framework. The convergence tolerances for energy, maximum force and maximum atomic displacement were set as 1.0×10^{-5} Ha, $0.002 \text{ Ha } \text{\AA}^{-1}$ and 0.005 \AA , respectively. The solvent effect was addressed using the COSMO implicit model of water. Since the Koopmans' approximation may lose its validity under the DFT framework, the HF method was applied to calculate the structural parameters using cc-pVTZ by virtue of the Gaussian 09W version D.01 software. The adsorption behavior of each compound on the metal surface was investigated using the Forcite module with MDS. The simulations of the interactions of the molecules with the Fe(110) surface were conducted in periodic boxes with the dimensions of $17.2 \text{ \AA} \times 16.2 \text{ \AA} \times 75.5 \text{ \AA}$ using two layers. The bottom Fe(110) surface was fabricated with a five-layer slab model and the top solvent layer was constructed with 222 H_2O , 1 organic molecule, 4 H^+ and 2 SO_4^{2-} , where a 30 \AA vacuum region was set to ensure the decoupling of the repeated slabs. The MDS were carried out under the conditions of 298 K, NVT ensemble, with a time step of 0.1 fs and simulation time of 500 ps.

4. Conclusions

A green corrosion inhibitor, ECSL, can be prepared from a plant waste, namely, cucumber leaves. It exhibits an excellent inhibition effect on the corrosion of carbon steel in $0.5 \text{ mol L}^{-1} \text{ H}_2\text{SO}_4$ solution, and its inhibition efficiency increases with increasing concentration. ECSL reduces both the cathodic and anodic reactions of carbon steel in H_2SO_4 solution. It is a mixed type corrosion inhibitor and its corrosion inhibition activities are attributed to the geometric coverage effect. Its interaction with the carbon steel surface is ascribed to spontaneous physical and chemical adsorption, which obeys the Langmuir adsorption law. The corrosion inhibition properties of ECSL are closely related to the unique molecular structures of its active components with many functional groups. The molecules can easily adsorb on the carbon steel surface using these functional groups as adsorption centers to form a protective layer, obstructing the corrosion medium and suppressing the corrosion of the carbon steel.

Supplementary Materials: The following supporting information can be downloaded at: <https://www.mdpi.com/article/10.3390/molecules27123826/s1>, Figure S1: GC–MS chromatogram of ECSL.

Author Contributions: Investigation, L.F. and S.Z.; Supervision, L.H.; Writing—original draft, L.F.; Visualization, R.P.; Writing—review and editing, G.H. and H.L.; Data curation, L.F., H.D. and G.H. All authors have read and agreed to the published version of the manuscript.

Funding: The APC was funded by Shandong Provincial Natural Science Foundation (No. ZR2019MEM046).

Data Availability Statement: Not Applicable.

Acknowledgments: The authors gratefully acknowledge the financial support from Shandong Provincial Natural Science Foundation (No. ZR2019MEM046), Shandong Society for Environmental Sciences Project (No. 202015), Doctoral Fund Project of Weifang University of Science and Technology (No. KJRC2022005 and No. KJRC2022006) and the open experimental project of Shandong Peninsula Engineering Research Center of Comprehensive Brine Utilization (No. 2018LS002). The authors also specially thank for the technique support in the chemical calculations and molecular simulations from National Supercomputer Center in Jinan and Institute of Metal Research, Chinese Academy of Sciences.

Conflicts of Interest: The authors declare no conflict of interest.

Sample Availability: Samples of ECSL is available from the authors.

References

1. Zhang, H.; Gao, K.; Yan, L.; Pang, X. Inhibition of the corrosion of X70 and Q235 steel in CO_2 -saturated brine by imidazoline-based inhibitor. *J. Electroanal. Chem.* **2017**, *791*, 83–94. [[CrossRef](#)]
2. Dagdag, O.; Safi, Z.; Erramli, H.; Cherkaoui, O.; Wazzan, N.; Guo, L.; Verma, C.; Ebenso, E.E.; El Harfi, A. Adsorption and anticorrosive behavior of aromatic epoxy monomers on carbon steel corrosion in acidic solution: Computational studies and sustained experimental studies. *RSC Adv.* **2019**, *9*, 14782–14796. [[CrossRef](#)]

3. Chauhan, D.S.; Quraishi, M.A.; Sorour, A.A.; Saha, S.K.; Banerjee, P. Triazole-modified chitosan: A biomacromolecule as a new environmentally benign corrosion inhibitor for carbon steel in a hydrochloric acid solution. *RSC Adv.* **2019**, *9*, 14990–15003. [[CrossRef](#)] [[PubMed](#)]
4. Dwivedi, D.; Lepková, K.; Becker, T. Carbon steel corrosion: A review of key surface properties and characterization methods. *RSC Adv.* **2017**, *7*, 4580–4610. [[CrossRef](#)]
5. Yang, X.; Li, F.; Zhang, W. 4-(Pyridin-4-yl)thiazol-2-amine as an efficient non-toxic inhibitor for mild steel in hydrochloric acid solutions. *RSC Adv.* **2019**, *9*, 10454–10464. [[CrossRef](#)] [[PubMed](#)]
6. Qiao, C.; Shen, L.; Hao, L.; Mu, X.; Dong, J.; Ke, W.; Liu, J.; Liu, B. Corrosion kinetics and patina evolution of galvanized steel in a simulated coastal-industrial atmosphere. *J. Mater. Res. Technol.* **2019**, *35*, 2345–2356. [[CrossRef](#)]
7. Wu, T.; Yan, M.; Yu, L.; Zhao, H.; Sun, C.; Yin, F.; Ke, W. Stress corrosion of pipeline steel under disbanded coating in a SRB-containing environment. *Corros. Sci.* **2019**, *157*, 518–530. [[CrossRef](#)]
8. Al-Shihry, S.S.; Sayed, A.R.; Abd El-lateef, H.M. Design and assessment of a novel poly(urethane-semicarbazides) containing thia-diazoles on the backbone of the polymers as inhibitors for steel pipelines corrosion in CO₂-saturated oilfield water. *J. Mol. Struct.* **2020**, *1201*, 127223. [[CrossRef](#)]
9. Kong, P.; Feng, H.; Chen, N.; Lu, Y.; Li, S.; Wang, P. Polyaniline/chitosan as a corrosion inhibitor for mild steel in acidic medium. *RSC Adv.* **2019**, *9*, 9211–9217. [[CrossRef](#)] [[PubMed](#)]
10. Lin, B.; Zuo, Y. Corrosion inhibition of carboxylate inhibitors with different alkylene chain lengths on carbon steel in an alkaline solution. *RSC Adv.* **2019**, *9*, 7065–7077. [[CrossRef](#)] [[PubMed](#)]
11. El Basiony, N.M.; Elgendy, A.; Nady, H.; Migahed, M.A.; Zaki, E.G. Adsorption characteristics and inhibition effect of two Schiff base compounds on corrosion of mild steel in 0.5 M HCl solution: Experimental, DFT studies, and Monte Carlo simulation. *RSC Adv.* **2019**, *9*, 10473–10485. [[CrossRef](#)]
12. Finšgar, M.; Jackson, J. Application of corrosion inhibitors for steels in acidic media for the oil and gas industry: A review. *Corros. Sci.* **2014**, *86*, 17–41. [[CrossRef](#)]
13. Ali, A.I.; Mahrous, Y.S. Corrosion inhibition of C-steel in acidic media from fruiting bodies of *Melia azedarach* L. extract and a synergistic Ni²⁺ additive. *RSC Adv.* **2017**, *7*, 23687–23698. [[CrossRef](#)]
14. Boudjellal, F.; Ouici, H.B.; Guendouzi, A.; Benali, O.; Sehmi, A. Experimental and theoretical approach to the corrosion inhibition of mild steel in acid medium by a newly synthesized pyrazole carbothioamide heterocycle. *J. Mol. Struct.* **2020**, *1199*, 127051. [[CrossRef](#)]
15. Hermoso-Diaz, I.A.; Foroosan, A.E.; Flores-De los Rios, J.P.; Landeros-Martinez, L.L.; Porcayo-Calderon, J.; Gonzalez-Rodriguez, J.G. Electrochemical and quantum chemical assessment of linoleic acid as a corrosion inhibitor for carbon steel in sulfuric acid solution. *J. Mol. Struct.* **2019**, *1197*, 535–546. [[CrossRef](#)]
16. Abdallah, Y.M.; Shalabi, K.; Bayoumy, N.M. Eco-friendly synthesis, biological activity and evaluation of some new pyridopyrimidinone derivatives as corrosion inhibitors for API 5L X52 carbon steel in 5% sulfamic acid medium. *J. Mol. Struct.* **2018**, *1171*, 658–671. [[CrossRef](#)]
17. Khalaf, M.M.; Tantawy, A.H.; Soliman, K.A.; Abd El-Lateef, H.M. Cationic gemini-surfactants based on waste cooking oil as new ‘green’ inhibitors for N80-steel corrosion in sulphuric acid: A combined empirical and theoretical approaches. *J. Mol. Struct.* **2020**, *1203*, 127442. [[CrossRef](#)]
18. Guo, L.; Obot, I.B.; Zheng, X.; Shen, X.; Qiang, Y.; Kaya, S.; Kaya, C. Theoretical insight into an empirical rule about organic corrosion inhibitors containing nitrogen, oxygen, and sulfur atoms. *Appl. Surf. Sci.* **2017**, *406*, 301–306. [[CrossRef](#)]
19. Tecuapa-Flores, E.D.; Turcio-Ortega, D.; Hernandez, J.G.; Huerta-Aguilar, C.A.; Thangarasu, P. The role of keto group in cyclic ligand 1,4,8,11-tetraazacyclotetradecane-5,7-dione as strong corrosion inhibitor for carbon steel surface: Experimental and theoretical studies. *J. Mol. Struct.* **2019**, *1189*, 131–145. [[CrossRef](#)]
20. Anupama, K.K.; Ramya, K.; Joseph, A. Electrochemical and computational aspects of surface interaction and corrosion inhibition of mild steel in hydrochloric acid by *Phyllanthus amarus* leaf extract (PAE). *J. Mol. Liq.* **2016**, *216*, 146–155. [[CrossRef](#)]
21. Feng, L.; Yang, H.; Cui, X.; Chen, D.; Li, G. Experimental and theoretical investigation on corrosion inhibitive properties of steel rebar by a newly designed environmentally friendly inhibitor formula. *RSC Adv.* **2018**, *8*, 6507–6518. [[CrossRef](#)]
22. Singh, A.; Ansari, K.R.; Quraishi, M.A.; Kaya, S. Theoretically and experimentally exploring the corrosion inhibition of N80 steel by pyrazol derivatives in simulated acidizing environment. *J. Mol. Struct.* **2020**, *1206*, 127685. [[CrossRef](#)]
23. Nathiya, R.S.; Raj, V. Evaluation of *Dryopteris cochleata* leaf extracts as green inhibitor for corrosion of aluminium in 1 M H₂SO₄. *Egypt. J. Pet.* **2017**, *26*, 313–323. [[CrossRef](#)]
24. Mehdipour, M.; Ramezanzadeh, B.; Arman, S.Y. Electrochemical noise investigation of Aloe plant extract as green inhibitor on the corrosion of stainless steel in 1 M H₂SO₄. *J. Ind. Eng. Chem.* **2015**, *21*, 318–327. [[CrossRef](#)]
25. Xhanari, K.; Finšgar, M.; Knez Hrnčič, M.; Maver, U.; Knez, Ž.; Seiti, B. Green corrosion inhibitors for aluminium and its alloys: A review. *RSC Adv.* **2017**, *7*, 27299–27330. [[CrossRef](#)]
26. Rodríguez-Gómez, F.J.; Valdelamar, M.P.; Vazquez, A.E.; Del Valle Perez, P.; Mata, R.; Miralrio, A.; Castro, M. Mycophenolic acid as a corrosion inhibitor of carbon steel in 3% wt. NaCl solution. An experimental and theoretical study. *J. Mol. Struct.* **2019**, *1183*, 168–181. [[CrossRef](#)]
27. Pitchaipillai, M.; Raj, K.; Balasubramanian, J.; Periakaruppan, P. Benevolent behavior of *Kleinia grandiflora* leaf extract as a green corrosion inhibitor for mild steel in sulfuric acid solution. *Int. J. Miner. Metall. Mater.* **2014**, *21*, 1083–1095. [[CrossRef](#)]

28. Li, X.; Deng, S.; Fu, H.; Xie, X. Synergistic inhibition effects of bamboo leaf extract/major components and iodide ion on the corrosion of steel in H₃PO₄ solution. *Corros. Sci.* **2014**, *78*, 29–42. [[CrossRef](#)]
29. Li, X.; Deng, S.; Li, N.; Xie, X. Inhibition effect of bamboo leaves extract on cold rolled steel in Cl₃CCOOH solution. *J. Mater. Res. Technol.* **2017**, *6*, 158–170. [[CrossRef](#)]
30. Chaubey, N.; Yadav, D.K.; Singh, V.K.; Quraishi, M.A. A comparative study of leaves extracts for corrosion inhibition effect on aluminium alloy in alkaline medium. *Ain Shams Eng. J.* **2017**, *8*, 673–682. [[CrossRef](#)]
31. Abiola, O.K.; Otaigbe, J.O.E. The effects of *Phyllanthus amarus* extract on corrosion and kinetics of corrosion process of aluminum in alkaline solution. *Corros. Sci.* **2009**, *51*, 2790–2793. [[CrossRef](#)]
32. Soltani, N.; Tavakkoli, N.; Khayatkashani, M.; Jalali, M.R.; Mosavizade, A. Green approach to corrosion inhibition of 304 stainless steel in hydrochloric acid solution by the extract of *Salvia officinalis* leaves. *Corros. Sci.* **2012**, *62*, 122–135. [[CrossRef](#)]
33. Gao, L.; Peng, S.; Gong, Z.; Chen, J. A combination of experiment and theoretical methods to study the novel and low-cost corrosion inhibitor 1-hydroxy-7-azabenzotriazole for mild steel in 1 M sulfuric acid. *RSC Adv.* **2018**, *8*, 38506–38516. [[CrossRef](#)]
34. Zhou, Y.; Zhang, P.; Su, L.; Fan, B.; Yan, F. One-step preparation and characterization of a Ce-La-Y ternary rare earth conversion coating on magnesium alloy AZ91D. *Mater. Lett.* **2021**, *304*, 130640. [[CrossRef](#)]
35. Singh, A.; Lin, Y.; Ebenso, E.E.; Liu, W.; Pan, J.; Huang, B. Ginkgo biloba fruit extract as an eco-friendly corrosion inhibitor for J55 steel in CO₂ saturated 3.5% NaCl solution. *J. Ind. Eng. Chem.* **2015**, *24*, 219–228. [[CrossRef](#)]
36. Li, L.; Zhang, X.; Lei, J.; He, J.; Zhang, S.; Pan, F. Adsorption and corrosion inhibition of *Osmanthus fragran* leaves extract on carbon steel. *Corros. Sci.* **2012**, *63*, 82–90. [[CrossRef](#)]
37. Elsaede, S.M.; El Tamany, E.S.H.; Ashour, H.; Zaki, E.G.; Khamis, E.A.; El Nagy, H.A. Corrosion and hydrogen evolution rate control for X-65 carbon steel based on chitosan polymeric ionic liquids: Experimental and quantum chemical studies. *RSC Adv.* **2018**, *8*, 37891–37904. [[CrossRef](#)]
38. Lebrini, M.; Robert, F.; Lecante, A.; Roos, C. Corrosion inhibition of C38 steel in 1M hydrochloric acid medium by alkaloids extract from *Oxandra asbeckii* plant. *Corros. Sci.* **2011**, *53*, 687–695. [[CrossRef](#)]
39. Gadow, H.S.; Motawea, M.M.; Elabbasy, H.M. Investigation of myrrh extract as a new corrosion inhibitor for α -brass in 3.5% NaCl solution polluted by 16 ppm sulfide. *RSC Adv.* **2017**, *7*, 29883–29898. [[CrossRef](#)]
40. Zehra, S.; Mobin, M.; Aslam, R.; Lgaz, H.; Chung, I.M. Assessment of biodegradable glycine and glutamic acid based ionic liquids as mild steel corrosion inhibitors in acid solution: An experimental and theoretical approach. *J. Mol. Struct.* **2021**, *1240*, 130505. [[CrossRef](#)]
41. Alrebh, A.; Rammal, M.B.; Omanovic, S. A pyridine derivative 2-(2-Methylaminoethyl)pyridine (MAEP) as a ‘green’ corrosion inhibitor for low-carbon steel in hydrochloric acid media. *J. Mol. Struct.* **2021**, *1238*, 130333. [[CrossRef](#)]
42. El Ibrahim, B.; Bazzi, L.; El Issami, S. The role of pH in corrosion inhibition of tin using the proline amino acid: Theoretical and experimental investigations. *RSC Adv.* **2020**, *10*, 29696–29704. [[CrossRef](#)]
43. Guo, L.; El Bakri, Y.; Anouar, E.H.; Tan, J.; Kaya, S.; Essassi, E.M. Multidimensional insights involving electrochemical and silicoinvestigation into the corrosion inhibition of newly synthesized pyrazolotriazole derivatives on carbon steel in a HCl solution. *RSC Adv.* **2019**, *9*, 34761–34771. [[CrossRef](#)]
44. El-Faham, A.; Osman, S.M.; Al-Lohedan, H.A.; El-Mahdy, G.A. Hydrazino-methoxy-1,3,5-triazine Derivatives’ Excellent Corrosion Organic Inhibitors of Steel in Acidic Chloride Solution. *Molecules* **2016**, *21*, 714. [[CrossRef](#)]
45. Umoren, S.A.; Li, Y.; Wang, F.H. Synergistic effect of iodide ion and polyacrylic acid on corrosion inhibition of iron in H₂SO₄ investigated by electrochemical techniques. *Corros. Sci.* **2010**, *52*, 2422–2429. [[CrossRef](#)]
46. Wang, X.; Yang, H.; Wang, F. An investigation of benzimidazole derivative as corrosion inhibitor for mild steel in different concentration HCl solutions. *Corros. Sci.* **2011**, *53*, 113–121. [[CrossRef](#)]
47. Moumeni, O.; Chafaa, S.; Kerkour, R.; Benbouguerra, K.; Chafai, N. Synthesis, structural and anticorrosion properties of diethyl (phenylamino) methyl phosphonate derivatives: Experimental and theoretical study. *J. Mol. Struct.* **2020**, *1206*, 127693. [[CrossRef](#)]
48. Madkour, L.H.; Kaya, S.; Guo, L.; Kaya, C. Quantum chemical calculations, molecular dynamic (MD) simulations and experimental studies of using some azo dyes as corrosion inhibitors for iron. Part 2: Bis-azo dye derivatives. *J. Mol. Struct.* **2018**, *1163*, 397–417. [[CrossRef](#)]
49. Feng, L.; Yang, H.; Wang, F. Inhibition Behavior of Ascorbic Benzoate for Steel Rebar in Alkaline Solution. *Acta Chim. Sin.* **2011**, *69*, 2359–2367.
50. Al-Amiery, A.A.; Al-Majedy, Y.K.; Kadhum, A.A.; Mohamad, A.B. New coumarin derivative as an eco-friendly inhibitor of corrosion of mild steel in Acid medium. *Molecules* **2014**, *20*, 366–383. [[CrossRef](#)]
51. Abdulazeez, I.; Khaled, M.; Al-Saadi, A.A. Impact of electron-withdrawing and electron-donating substituents on the corrosion inhibitive properties of benzimidazole derivatives: A quantum chemical study. *J. Mol. Struct.* **2019**, *1196*, 348–355. [[CrossRef](#)]
52. Gece, G. The use of quantum chemical methods in corrosion inhibitor studies. *Corros. Sci.* **2008**, *50*, 2981–2992. [[CrossRef](#)]
53. Guo, L.; Qi, C.; Zheng, X.; Zhang, R.; Shen, X.; Kaya, S. Toward understanding the adsorption mechanism of large size organic corrosion inhibitors on an Fe(110) surface using the DFTB method. *RSC Adv.* **2017**, *7*, 29042–29050. [[CrossRef](#)]
54. Kokalj, A. On the HSAB based estimate of charge transfer between adsorbates and metal surfaces. *Chem. Phys.* **2012**, *393*, 1–12. [[CrossRef](#)]
55. El-Hendawy, M.M.; Kamel, A.M.; Mohamed, M.M.A. The anti-corrosive behavior of benzo-fused N-heterocycles: An in silico study toward developing organic corrosion inhibitors. *Phys. Chem. Chem. Phys.* **2022**, *24*, 743–756. [[CrossRef](#)]

56. Stowasser, R.; Hoffmann, R. What Do the Kohn-Sham Orbitals and Eigenvalues Mean? *J. Am. Chem. Soc.* **1999**, *14*, 3414–3420. [[CrossRef](#)]
57. Awad, M.K.; Mustafa, M.R.; Elnga, M.M.A. Computational simulation of the molecular structure of some triazoles as inhibitors for the corrosion of metal surface. *J. Mol. Struct. Theochem* **2010**, *959*, 66–74. [[CrossRef](#)]
58. Zhang, W.; Nie, B.; Wang, M.; Shi, S.; Gong, L.; Gong, W.; Pang, H.; Liu, X.; Li, B.; Feng, Y.; et al. Chemically modified resveratrol as green corrosion inhibitor for Q235 steel: Electrochemical, SEM, UV and DFT studies. *J. Mol. Liq.* **2021**, *343*, 117672. [[CrossRef](#)]
59. Bhardwaj, N.; Sharma, P.; Guo, L.; Dagdag, O.; Kumar, V. Molecular dynamic simulation and Quantum chemical calculation of phytochemicals present in *Beta vulgaris* and electrochemical behaviour of *Beta vulgaris* peel extract as green corrosion inhibitor for stainless steel (SS-410) in acidic medium. *Colloids Surf. A Physicochem. Eng. Asp.* **2022**, *632*, 127707. [[CrossRef](#)]
60. Derry, G.N.; Kern, M.E.; Worth, E.H. Recommended values of clean metal surface work functions. *J. Vac. Sci. Technol. A* **2015**, *33*, 060801. [[CrossRef](#)]
61. Kobzar, Y.L.; Fatyeyeva, K. Ionic liquids as green and sustainable steel corrosion inhibitors: Recent developments *Chem. Eng. J.* **2021**, *425*, 131480. [[CrossRef](#)]
62. Guimarães, T.A.S.; da Cunha, J.N.; de Oliveira, G.A.; da Silva, T.U.; de Oliveira, S.M.; de Araújo, J.R.; Machado, S.d.P.; D'Elia, E.; Rezende, M.J.C. Nitrogenated derivatives of furfural as green corrosion inhibitors for mild steel in HCl solution. *J. Mater. Res. Technol.* **2020**, *9*, 7104–7122. [[CrossRef](#)]
63. About, S.; Hsissou, R.; Erramli, H.; Chebabe, D.; Salim, R.; Kaya, S.; Hajjaji, N. Gravimetric, electrochemical and theoretical study, and surface analysis of novel epoxy resin as corrosion inhibitor of carbon steel in 0.5 M H₂SO₄ solution. *J. Mol. Struct.* **2021**, *1245*, 131014. [[CrossRef](#)]
64. Sayin, K.; Karakaş, D. Quantum chemical studies on the some inorganic corrosion inhibitors. *Corros. Sci.* **2013**, *77*, 37–45. [[CrossRef](#)]
65. Obot, I.B.; Kaya, S.; Kaya, C.; Tüzün, B. Density Functional Theory (DFT) modeling and Monte Carlo simulation assessment of inhibition performance of some carbohydrazide Schiff bases for steel corrosion. *Physica E* **2016**, *80*, 82–90. [[CrossRef](#)]
66. Corzo, H.H.; Galano, A.; Dolgounitcheva, O.; Zakrzewski, V.G.; Ortiz, J.V. NR2 and P3+: Accurate, Efficient Electron-Propagator Methods for Calculating Valence, Vertical Ionization Energies of Closed-Shell Molecules. *J. Phys. Chem. A* **2015**, *119*, 8813–8821. [[CrossRef](#)]
67. Olasunkanmi, L.O.; Obot, I.B.; Kabanda, M.M.; Ebenso, E.E. Some Quinoxalin-6-yl Derivatives as Corrosion Inhibitors for Mild Steel in Hydrochloric Acid: Experimental and Theoretical Studies. *J. Phys. Chem. C* **2015**, *119*, 16004–16019. [[CrossRef](#)]
68. Martinez, S.; Valek, L.; Oslaković, I.S. Adsorption of Organic Anions on Low-Carbon Steel in Saturated Ca(OH)₂ and the HSAB Principle. *J. Electrochem. Soc.* **2007**, *154*, C671–C677. [[CrossRef](#)]
69. Durnie, W.; Marco, R.D.; Jefferson, A.; Kinsella, B. Development of a Structure-Activity Relationship for Oil Field Corrosion Inhibitors. *J. Electrochem. Soc.* **1999**, *146*, 1751–1756. [[CrossRef](#)]
70. Gao, Y.; Chen, J.; Lei, L.; Yang, H.; Zhu, Y. The application of acid-base theory in corrosion processes. *Corros. Sci. Prot. Technol.* **2000**, *12*, 319–322.
71. Chauhan, D.S.; Verma, C.; Quraishi, M.A. Molecular structural aspects of organic corrosion inhibitors: Experimental and computational insights. *J. Mol. Struct.* **2021**, *1227*, 129374. [[CrossRef](#)]
72. Berdimurodov, E.; Kholikov, A.; Akbarov, K.; Guo, L.; Kaya, S.; Katin, K.P.; Verma, D.K.; Rbaa, M.; Dagdag, O.; Haldhar, R. Novel gossypol-indole modification as a green corrosion inhibitor for low-carbon steel in aggressive alkaline-saline solution. *Colloids Surf. A Physicochem. Eng. Asp.* **2022**, *637*, 128207. [[CrossRef](#)]
73. Migahed, M.A.; Zaki, E.G.; Shaban, M.M. Corrosion control in the tubing steel of oil wells during matrix acidizing operations. *RSC Adv.* **2016**, *6*, 71384–71396. [[CrossRef](#)]
74. Mazlan, N.; Jumbri, K.; Azlan Kassim, M.; Abdul Wahab, R.; Basyaruddin Abdul Rahman, M. Density functional theory and molecular dynamics simulation studies of bio-based fatty hydrazide-corrosion inhibitors on Fe (110) in acidic media. *J. Mol. Liq.* **2022**, *347*, 118321. [[CrossRef](#)]